Supplementary materials for:

The 2022 M_W 6.0 Gölyaka-Düzce earthquake: an example of a medium size earthquake in a fault zone early in its seismic cycle

by

P. Martínez-Garzón[1], D. Becker[1], J. Jara[2], X., Chen[1], G. Kwiatek[1] and M. Bohnhoff[1,3]

[1] Section 4.2, Helmholtz Centre Potsdam GFZ German Research Centre for Geosciences, Potsdam, Germany.

[2]Section 2.6, Helmholtz Centre Potsdam GFZ German Research Centre for Geosciences, Potsdam, Germany.

[3] Free University Berlin, Institute of Geological Sciences, Berlin, Germany

Corresponding author: Patricia Martínez-Garzón (patricia@gfz-potsdam.de)

Supplementary Materials:

Text S1. Additional details on the processing of the catalog of absolute locations.

We calculated event locations by employing the probabilistic location software NLLoc (Lomax et al., 2000; 2009). Here, only events with a minimum of 6 P- and/or S- picks were further processed. The local 1-D velocity model from Bulut et al. (2007) was employed assuming a constant v_p/v_s ratio of 1.73. The search area encompassed a 400 km x 200 km region centered around the mainshock epicenter. In the following, we refer to this refined catalog as the "*catalog of absolute locations*".

Inspection of event waveforms and station residuals indicated that three accelerometers (stations 8105, 8106 and 8108) displayed an incorrect time base. These stations were then removed from further processing as an attempt to correct the time base using waveform cross-correlations of P-onsets of teleseismic events did not result in an improvement of the station residuals. Furthermore, inspection of origin times of an initial NLLoc run using all events from the catalog of detections revealed some events with nearly identical origin times. A visual inspection of the picks associated by GaMMA revealed that those were artificially created duplicates by separating phases belonging to the same event into two distinct events. To check

whether this was caused by the accelerometer stations with incorrect time base, we re-ran the GaMMA association without stations 8105, 8106 and 8108. However, the separation of phases belonging to the same event into two separate events still remained in more than 200 instances. Thus, this seemed to be caused by the specific station geometry of our study with one tight cluster of accelerometer stations within a seismometer network of much larger inter-station spacing as in most cases (but not in all) accelerometer stations were grouped into one event and seismometer stations in another event by GaMMA. We subsequently merged all events with an origin time difference of less than 5 s (249 cases in total).

Text S2: Analysis of Empirical Green's functions

Besides utilizing the initial P-wave segments to analyze the earthquake directivity, we also tried to resolve the apparent source time function using Empirical Green's function method (Hartzell, 1978; Ammon et al., 1993, Tan 2010; Abercrombie 2017). As a preliminary investigation, four M4-5 earthquakes near the Gölyaka-Düzce mainshock were tested as the EGFs to deconvolve the path and site effects from the mainshock waveforms (Table S3). The four EGF candidates were within an epicentral distance of 10 km from the mainshock according to the AFAD catalog, and had some variations on depth. We selected the relative larger events as they are recorded by more stations with better coverage of azimuthal angles and have available focal mechanism solutions. Only the first 5 s of the P wave were here used, as directivity features are mostly present in the early part of the seismogram.

Despite using a handful of EGF events to deconvolve propagation effects, the obtained apparent source time functions did not provide convincing proofs for directivity. This is partially conditioned on a limited number of stations for which a clear source time function could be extracted from the EGF deconvolution. It may be that the tested events as EGFs, despite sharing generally similar polarity patterns, did not strictly fulfill the requirements for EGFs. For example, the actual focal mechanism may not correspond to the mechanism of the mainshock, or the EGFs and mainshock were not occurring exactly at the same location. In addition, we only tested four M4-5 events as EGFs, for which the magnitude difference with respect to the mainshock may not be distinct. One possibility is that the tested EGF events occurred on the Düzce fault, while the mainshock occurred in the Karadere fault, hence not sharing common path and source properties.

Table S1: Compilation of fault plane parameters from different moment tensor solutions calculated by different agencies for the 2022 M_W 6.0 Gölkaya-Düzce earthquake.

	Strike 1	Dip 1	Rake 1	Strike 2	Dip 2	Rake 2
KOERI	167	88	-16	257	73	-178
USGS	160	63	-19	259	73	-152
AUST	346	88	32	255	82	178
IPGP	165	82	-19	257	72	-172
GEOFON	345	80	-16	78	74	-169

Table S2. Inferred parameters for GR law with their respective uncertainties for AFAD and KOERI catalogs. Here, A is a normalization constant (see Eq 3 from main text), b is the b-value from the Gutenberg-Richter relation, and μ and σ correspond to the mean and standard deviation of the probability distribution function of the error function, respectively (see Eq 4 from the main text).

Catalog	$A \times 10^7$	b	$\hat{\mu}$	$\hat{\sigma}$
AFAD	1.965 ± 0.108	1.19 ± 0.01	2.746 ± 0.005	0.325 ± 0.001
KOERI	6.154 ± 0.813	1.14 ± 0.01	3.276 ± 0.003	0.422 ± 0.001

Table S3: List of earthquakes tested as potential EGFs (earthquake information from AFAD catalog)

Event	Time	Longitude	Latitude	Depth	Magnitude (Mw)
E1	2022-11-27 03:57:46	31.048	40.846	9.52	4.3
E2	2022-11-23 03:50:58	30.957	40.789	9.45	4.3
E3	2021-11-17 12:57:18	31.035	40.7981	7.11	4.3
E4	2021-11-17 12:40:15	31.0316	40.844	18.29	5

References

Abercrombie, R. E., Poli, P., & Bannister, S. (2017). Earthquake directivity, orientation, and stress drop within the subducting plate at the Hikurangi margin, New Zealand. Journal of Geophysical Research: Solid Earth, 122, 10,176–10,188. https://doi.org/10.1002/ 2017JB014935.

Ammon, A. J., A. A. Velasco, and T. Lay (1993). Rapid estimation of rupture directivity—Application to the 1992 Landers (Ms 7:4) and Cape Mendocino (Ms 7:2), California earthquakes, Geophys. Res. Lett. 20, no. 2, 97–100.

Hartzell, S. H. (1978). Earthquake aftershocks as Green's functions, Geophys. Res. Lett. 5, no. 1, 1–4.

Tan, Y., & Helmberger, D. (2010). Rupture directivity characteristics of the 2003 Big Bear sequence. *Bulletin of the Seismological Society of America*, *100*(3), 1089-1106.

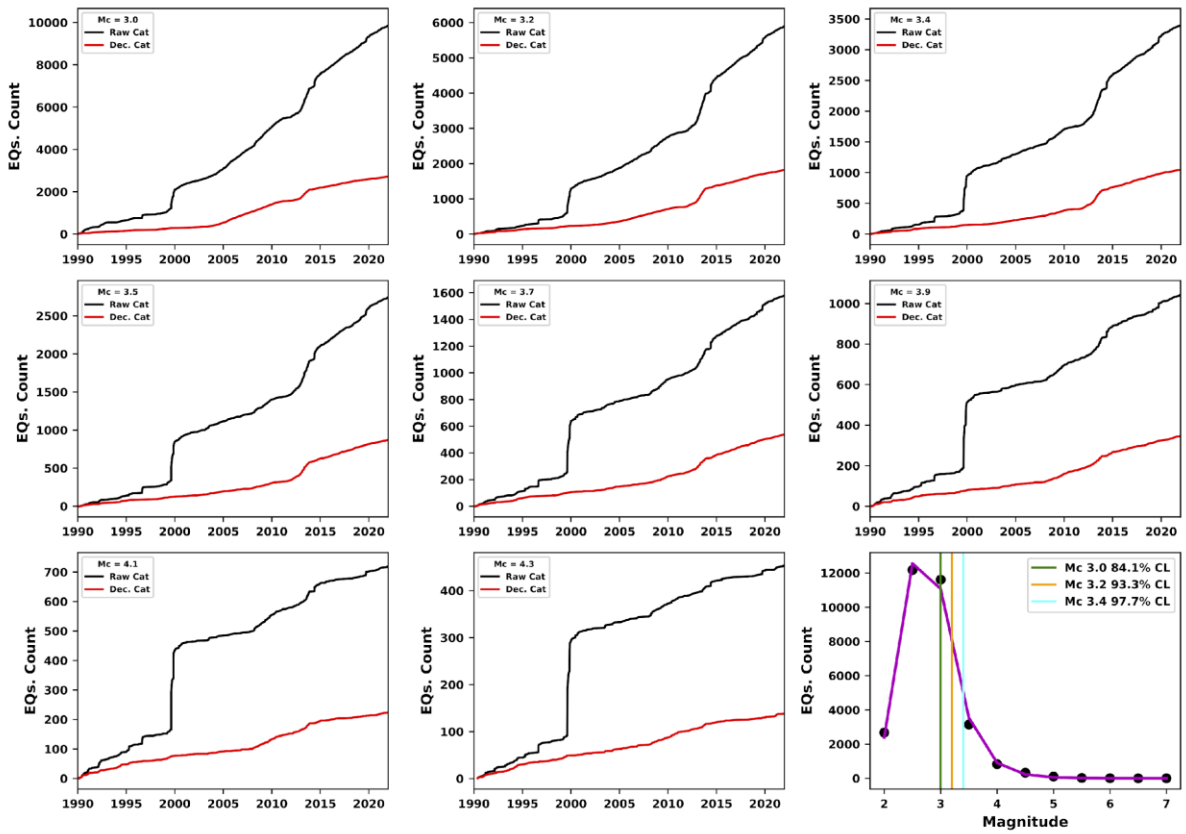

Figure S1: Comparison between raw (black lines) and declustered catalogs (red lines) for different Mc (3.0, 3.2, 3.4, 3.5, 3.7, 3.9, 4.1, and 4.3) for AFAD catalog. On bottom right, function and fit where the GR law is estimated.

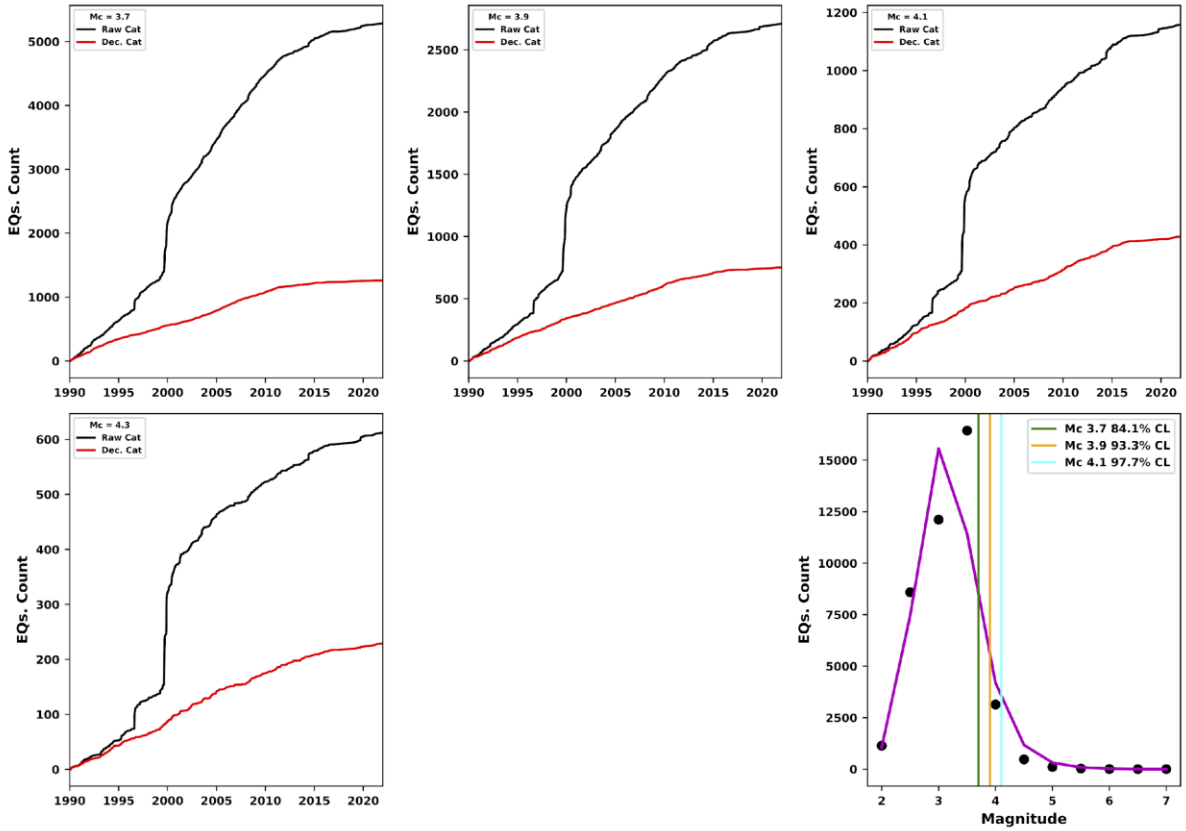

Figure S2: Comparison between raw (black lines) and declustered catalogs (red lines) for different Mc (3.7, 3.9, 4.1, and 4.3) for KOERI catalog. On bottom right, function and fit where the GR law is estimated.

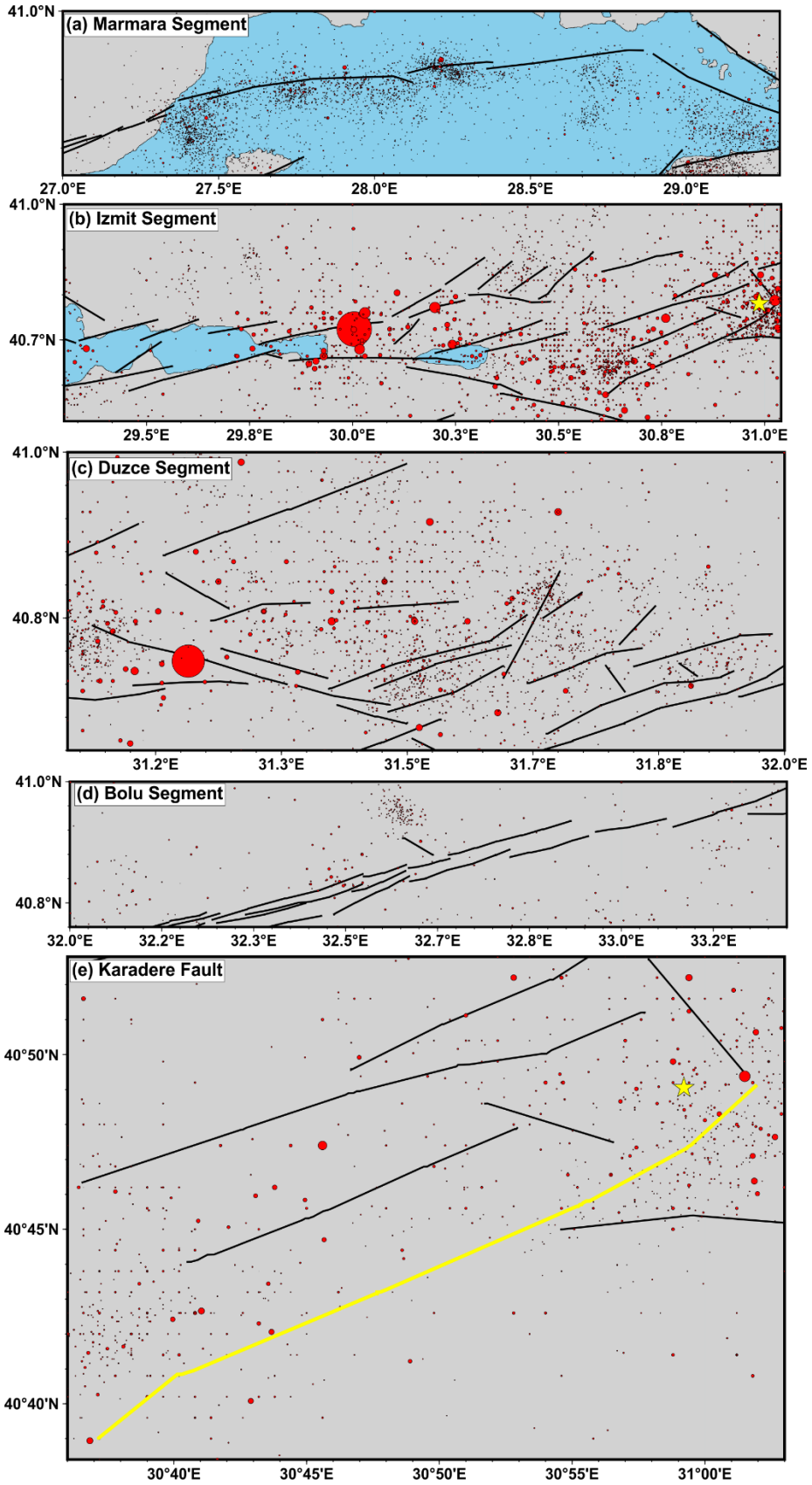

Figure S3: Spatial distribution of the seismic events (1990 to 30/11/2022) from AFAD catalog for each of the regions analyzed in sections 2.1 and 3.1. (a) Marmara fault segment, (b) Izmit Segment, (c) Düzce segment, (d) Bolu segment, (e) Karadere segment.

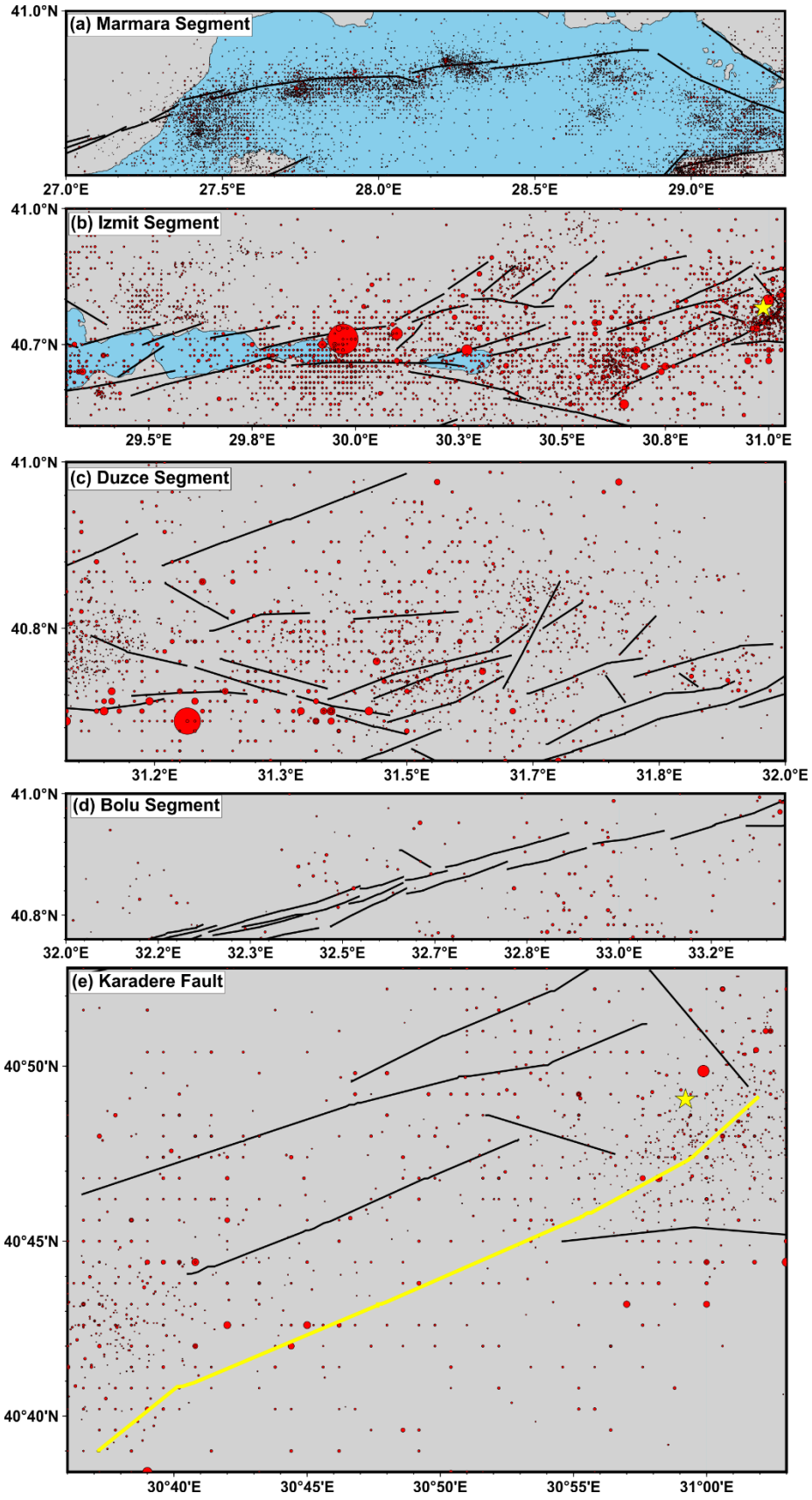

Figure S4: Same as Figure S3 but using the KOERI seismicity catalog.

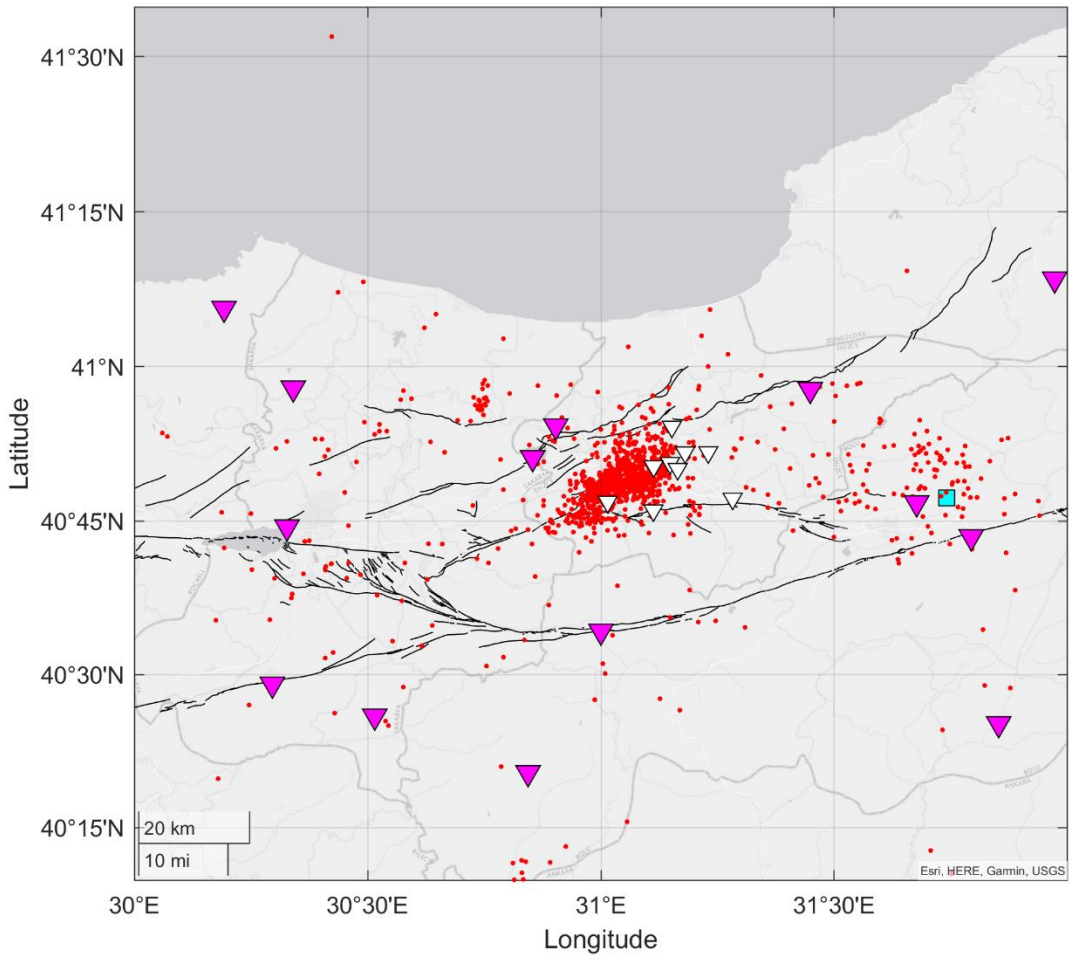

Figure S5: Spatial distribution of the seismic events included in the catalog of absolute locations.

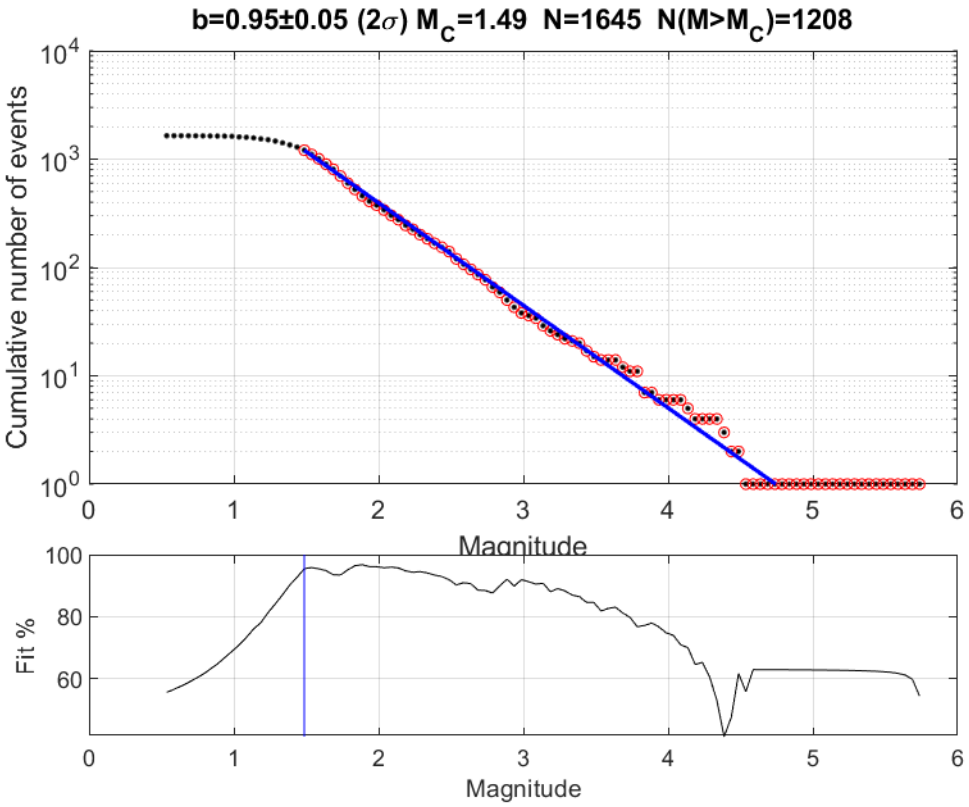

Figure S6: Magnitude-frequency cumulative distribution of earthquake magnitudes (black dots). The b-value was estimated using maximum likelihood and goodness of fit method (Wiemer and Wyss, 2000) assuming that 95% of data above magnitude of completeness is explained by the Gutenberg-Richter power law (blue line).

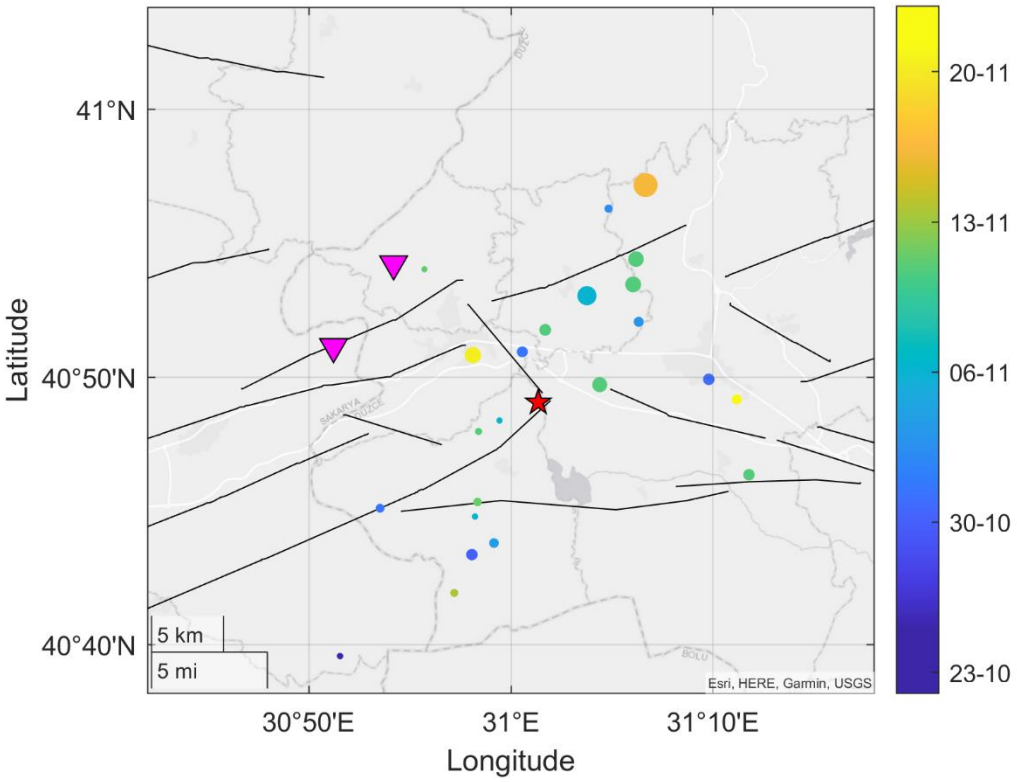

Figure S7: Spatio-temporal evolution of the seismic events that occurred in the vicinity of the future M_W 6.0 Gölyaka-Düzce earthquake. Color and size of the circles is encoded with the origin time and the magnitude of the events, respectively. Red star represents the epicenter of the M_W 6.0 Gölyaka-Düzce earthquake. Pink downward triangles represent seismic stations.

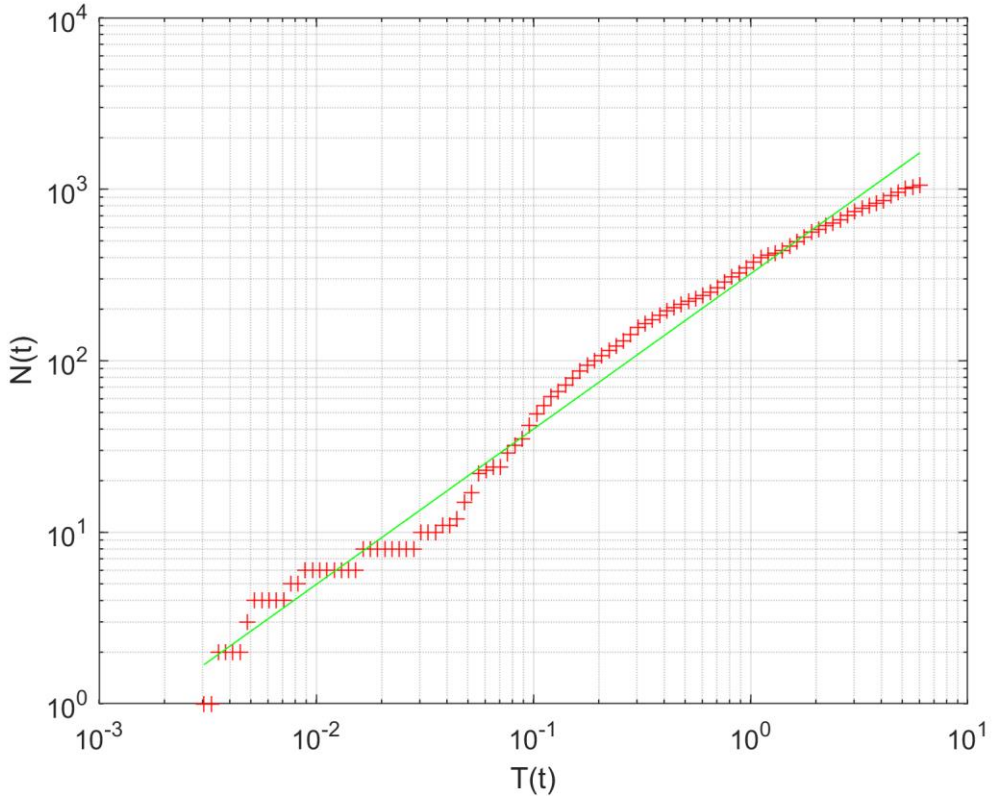

Figure S8. Frequency distribution of time differences between aftershocks and the M_W 6.0 event on Nov 23th, 2022. T(t): Temporal difference of each aftershock with respect to the mainshock. N(t): Number of events. Red crosses represent the data from dividing the distribution of aftershocks into 100 bins. Green line represents the fitting of the Omori's Law.

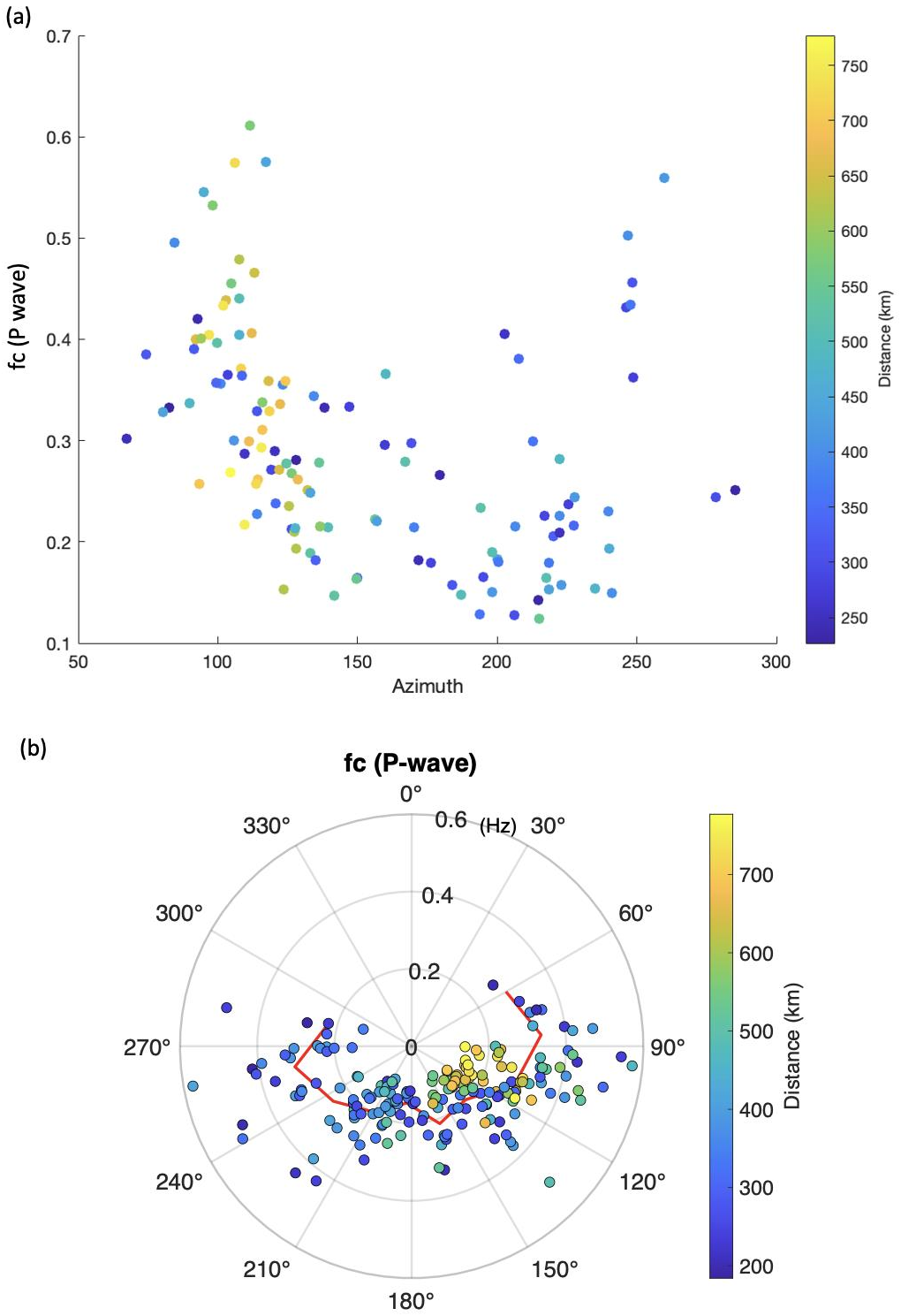

Figure S9. Corner frequencies from P-wave spectra obtained in this analysis as a function of their azimuthal orientation from the mainshock in (a) Cartesian coordinate system and (b) polar coordinate system. Symbols are encoded with the epicentral distance. The background red line shows the median value in every 25° interval.